

Numerical simulation and analysis of the flow in a two-staged axial fan

J Q Xu ¹, H S Dou^{*1}, H X Jia¹, X P Chen¹, Y K Wei¹ and M W Dong²

¹ Faculty of Mechanical Engineering and Automation, Zhejiang Sci-Tech University, Hangzhou 310018, China

² Zhejiang Shuangyang Fan CO. Ltd. Shangyu, 312300, China

*Email: huashudou@yahoo.com

Abstract. In this paper, numerical simulation was performed for the internal three-dimensional turbulent flow field in the two-stage axial fan using steady three-dimensional in-compressible Navier-Stokes equations coupled with the Realizable turbulent model. The numerical simulation results of the steady analysis were combined with the flow characteristics of two-staged axial fan, the influence of the mutual effect between the blade and the vane on the flow of the two inter-stages was analyzed emphatically. This paper studied how the flow field distribution in inter-stage is influenced by the wake interaction and potential flow interaction of mutual effect in the impeller-vane inter-stage and the vane-impeller inter-stage. The results showed that: Relatively, wake interaction has an advantage over potential flow interaction in the impeller-vane inter-stage; potential flow interaction has an advantage over wake interaction in the vane-impeller inter-stage. In other words, distribution of flow field in the two inter-stages is determined by the rotating component.

1. Introduction

In recent years, the rotor-stator interaction phenomenon of the axial fan has attracted a lot of researchers. The aerodynamic performance and the strength of structure such as the efficiency, operating range, the running stability and etc. And all the performance of an axial fan is influenced by the relative motion between the blade and guide blade. The rotor-stator interaction in fluid machine mainly contains the wake interaction in the upstream row, channel and gap and the in-viscid potential flow interaction in the blade and vane [1]. Studying the influence of the different aspects of the rotor-stator interaction can be helpful to design of axial fan and can be improve aerodynamic performance of the fan.

Many scholars have done a lot of research. In the field of experiment, Wang et al [2] used dynamic pressure sensor to measure the upstream vane rotor blade wake effects on unsteady surface pressure spectral characteristics. The measurement results showed that the trailing edge separation flow generated by the pressure fluctuation spectrum contains the upstream blade wake passing frequency and its harmonics component. Wu et al [3] used particle image velocity on static wake and dynamic blades mutual interference flow field with experimental measurements it is concluded that with the effect of the stator wake, the fluctuations of the inlet flow angle on rotor-blade become larger, resulting in the intake airflow uneven. The passage [4] used the hot-film to do the research on the flow field of rotor-stator interference and the pressure fluctuation of the axial turbo-machinery. The study of the experiment showed that the influence of the stator wake on the downstream of the rotor blade



under two different situations of static and dynamic axial clearance. The passage [5] studied vane wake's effects on the blade row between the quasi-orthogonal plane flow structure, under the condition of the vanes and the rotor axial distance changes. In the field of numerical simulation, Mao et al [6] studied the influence of wake and potential effects on the dynamic and static blade surface aerodynamic load. The results showed that upstream dynamic blade wake had great impact on the generation and transportation of the blade boundary layer flow losses. Qi et al [7] studied the influence of the rotor-stator interaction on the aerodynamic performance of the movement of axial turbine stages. Yang et al [8] analysed superposition effect of the potential flow and wake interference of the flow compressor. As for the analysis of the flow the fluid mechanical inter-stages. Xiao and Wang [9-10] from Huazhong University of Science and Technology have done the numerical simulation on the mutual interference between rotating axial flow fan stages, the conclusion that in the counter rotating axial flow fan, wake interference of the front stage impeller is stronger than that of the end stage impeller. Yang et al [11] from Jiangsu University had done the large eddy simulation on the axial flow band with the guide vane.

The former mainly studied the rotor-stator interaction from the following aspects: inter-stage spacing, number of the impeller blades and vanes blades, and the relative location of static and dynamic blades. The majority focused on single-stage pump or fan and mainly discussed of the rotor-stator interaction influence in the flow channel. But the numerical simulation about the rotor-stator interaction of two-stage axial fan with vanes in the middle is few.

In this paper, numerical simulation is performed for the internal three-dimensional turbulent flow field in the two-stage axial fan using steady three-dimensional in-compressible Navier-Stokes equations coupled with the Realizable turbulent model, the influence of the mutual effect between the blade and the vane on the flow of the two stages is analyzed emphatically. This paper studied how the flow field distribution in stage is influenced by the wake interaction and potential flow interaction of mutual effect in the impeller-vane stage and the vane-impeller stage. It also provide reliable information to the further research of wake and potential flow interaction in impeller and vane.

2. Governing equation and numerical method

2.1. Geometric model

The two-stage axial fan with vane is produced by a Zhe Jiang Company. The main structural features show that its impeller design considered the pressure loss changing along the radial direction. The value of the chord length of the blade, adjustable mounting angle and curvature of the center line of the plate-shaped blades are changing according to certain rules. Its characteristics are that the maximum efficiency of point is consistent with the design point. The two-stage axial fan axial fan can not only show the large flow characteristics, but also improve the pressure head of the axial fan through gas working to impellers.

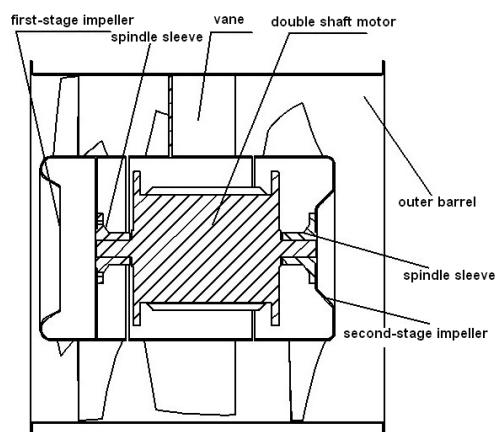


Figure 1. Two-staged Axial Fan structure diagram

The fan mainly contains impeller, guide vane motor, and the outer cylinder. The specific circumstances of the structure are shown in Figure 1. There are six blades in the first stage, nine blades in the guide vane, and five blades in the second-stage. Specific parameters are shown in Table 1.

Table 1. Main parameters of axial fan.

parameters	values
Hub ratio	0.54
Blade number of first-stage fan	6
Blade number of second-stage fan	5
Blade numbers of vane	9
Rotational speed (r/min)	960
Volume rate of flow (m^3/h)	68000
total pressure (pa)	710
Total pressure efficiency (%)	52

2.2. Computational domain mesh

Numerical Simulation used mesh, as shown in Figure 2. For clearly show the axial fan mesh, here were omitted inlet fluid computational domain and outlet fluid computational domain. Each computational domain was generated the appropriate distribution of mesh nodes and appropriate size of mesh separately, for mesh quality control, improve accuracy in numerical simulation. Entire two-staged axial fan was divided into five computational domain, including inlet, first-stage impeller, vane impeller, second-stage impeller and outlet computational domain. Mesh number of each part were 0.19 millions, 4.5 million, 1.5 millions, 3.6 million and 0.25 million, giving a total of 10.04 million. Inlet domain, vane domain, outlet domain were static. First-stage impeller domain and second-stage impeller domain were rotating.

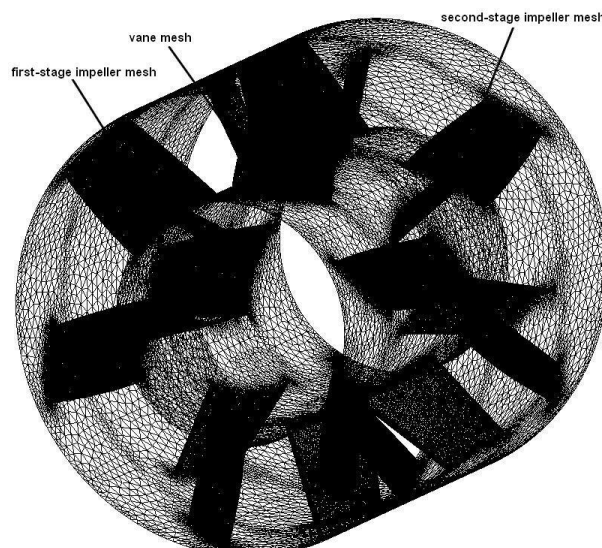


Figure 2. Computational mesh of the axial fan

2.3. Computational method and boundary conditions

The inlet boundary conditions was mass flow inlet on design condition, the outlet boundary conditions was an atmospheric pressure. Turbulent kinetic energy and turbulent kinetic energy dissipation rate

was estimated by using empirical formula in inlet and outlet. In this model, governing equation was dispersed using finite volume method in the space, Steady computing used Second order upwind difference, The method of solving equations used SIMPLE algorithm. Computational fluid is 25°C of air. The outlet boundary conditions was no slip boundary condition [12], Near-wall region used the standard wall function. Using this turbulence model could get better numerical simulation results for the problem of involving rotating, adverse pressure gradient, boundary-layer separation, reflux, and secondary flow.

2.4. Governing equation

Governing equation is three-dimensional in-incompressible Navier – Stokes equations:

$$\begin{cases} \frac{\partial \bar{u}_i}{\partial x_i} = 0 \\ \rho u_j \frac{\partial \bar{u}_i}{\partial x_j} = \rho F_i - \frac{\partial \bar{p}}{\partial x_i} + \mu \frac{\partial^2 \bar{u}_i}{\partial x_j \partial x_j} - \rho \frac{\partial}{\partial x_j} (\bar{u}_i \bar{u}_j) \end{cases} \quad (1)$$

Turbulence model was Realizable k-ε model. This model was proposed by Shih et al [13] in 1995. Constraint equation is as follows:

$$\frac{\partial(\rho k)}{\partial t} + \frac{\partial(\rho k u_j)}{\partial x_j} = \frac{\partial}{\partial x_j} \left[\left(\mu + \frac{\mu_t}{\sigma_k} \right) \frac{\partial k}{\partial x_j} \right] + \rho(P_k - \varepsilon) \quad (2)$$

$$\frac{\partial(\rho \varepsilon)}{\partial t} + \frac{\partial(\rho \varepsilon u_j)}{\partial x_j} = \frac{\partial}{\partial x_j} \left[\left(\mu + \frac{\mu_t}{\sigma_\varepsilon} \right) \frac{\partial \varepsilon}{\partial x_j} \right] + \rho C_1 E \varepsilon - \rho C_2 \frac{\varepsilon^2}{k + \sqrt{\nu \varepsilon}} \quad (3)$$

Among:

$$C_1 = \max \left(0.43, \frac{\eta}{\eta + 5} \right)$$

$$\eta = \left(2 E_{ij} \cdot E_{ij} \right)^{1/2} \frac{k}{\varepsilon}$$

$$E_{ij} = \frac{1}{2} \left(\frac{\partial u_i}{\partial x_j} + \frac{\partial u_j}{\partial x_i} \right)$$

Constant in the equation: $\sigma_k = 1.0$, $\sigma_\varepsilon = 1.2$, $C_2 = 1.9$

2.5. Mesh independent verification

Computational mesh was independent verification on design condition of the two-stage axial fan. Three sets of mesh were designed; the mesh numbers were 8.06 million, 10.04 million and 12.03 million. Total pressure is shown in Figure 3 at the different number of mesh. From the figure, the total pressure is preferably Convergence on design condition. The total variation range of total pressure was about 3%. It meets mesh-independent; 10.04 million number of computational Mesh was selected in this paper.

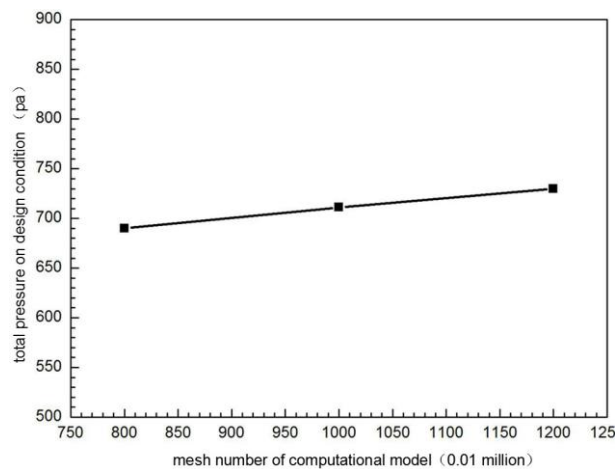


Figure 3. Mesh independent verification

3. Calculation results and discussions

The three dimensional flow in a two-staged axial fan has its inherent characteristic of non constant. Since a two-staged axial fan is composed of two impellers and a middle guide vane, there are two stages: the impeller-vane inter-stage and the vane-impeller inter-stage. Because of the rotor-stator interaction, the flow of the two-staged axial fan is very complex. This paper will focus on the influence of flow field in inter-stage by the wake and the potential flow.

To analyze how the distribution of flow field in inter-stage is influenced by the wake interaction and the potential flow interaction of mutual effect in the impeller-vane inter-stage and the vane-impeller inter-stage, axial distance in two inter-stages is divided into 4 equal parts, got A1、A2、A3、A4 and B1、B2、B3、B4 sections, as shown in Figure 4.

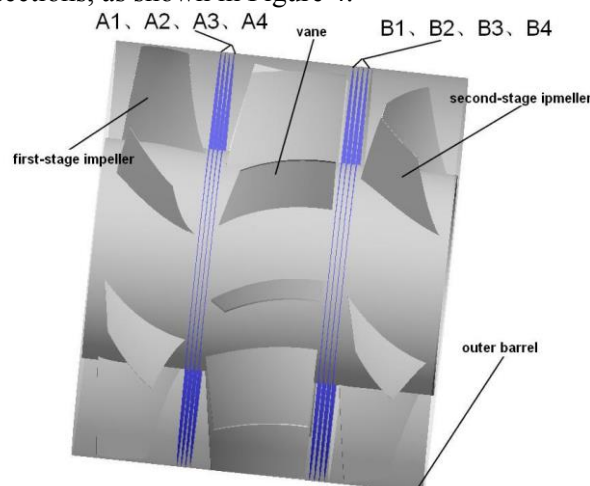


Figure 4. Sectional position schematic diagram

3.1. Analysis of the pressure, velocity and vorticity distribution of the axis in the two inter-stage

In order to study the fluid flow of the impeller-vane inter-stage and the vane-impeller inter-stage, this section analyzes and studies the total pressure, static pressure, velocity and vorticity of the fluid flowing through two stages.

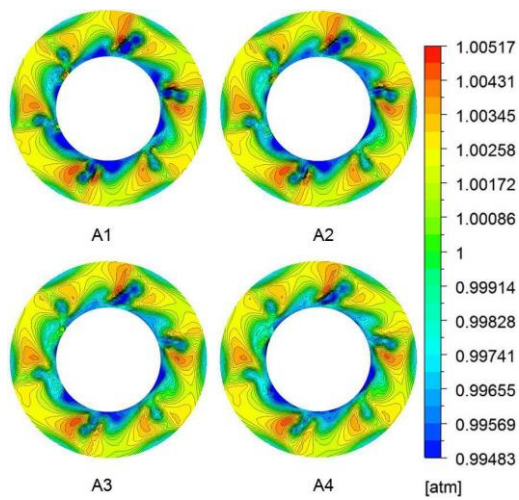


Figure 5. Total pressure distribution in the impeller-vane inter-stage.

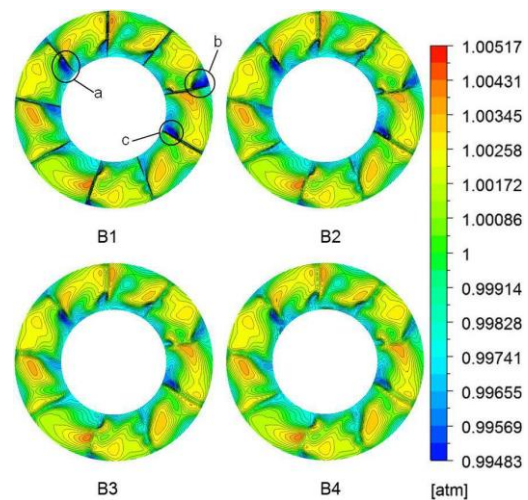


Figure 6. Total pressure distribution in the vane-impeller inter-stage.

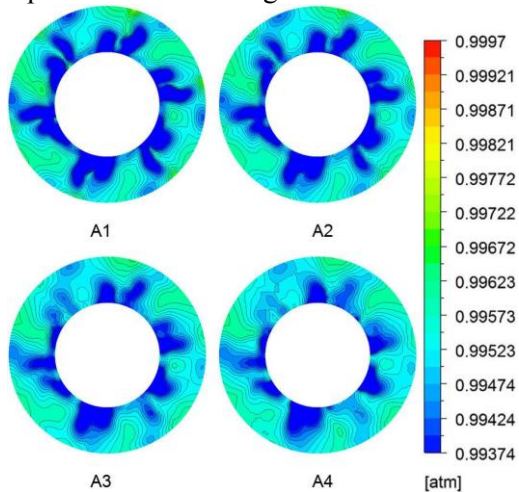


Figure 7. Static pressure distribution in the impeller-vane inter-stage.

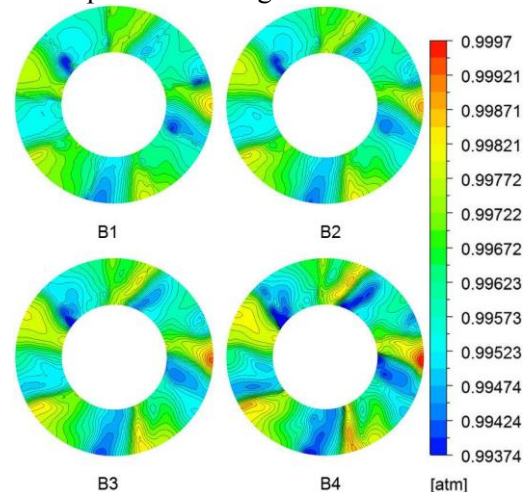


Figure 8. Static pressure distribution in the vane-impeller inter-stage.

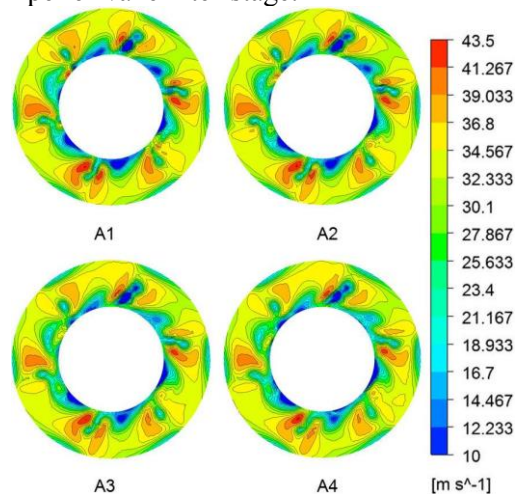


Figure 9. Velocity distribution in the impeller- vane inter-stage.

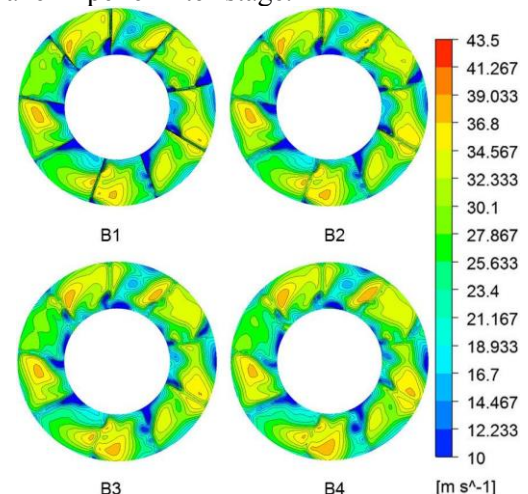


Figure 10. Velocity distribution in the vane-impeller inter-stage.

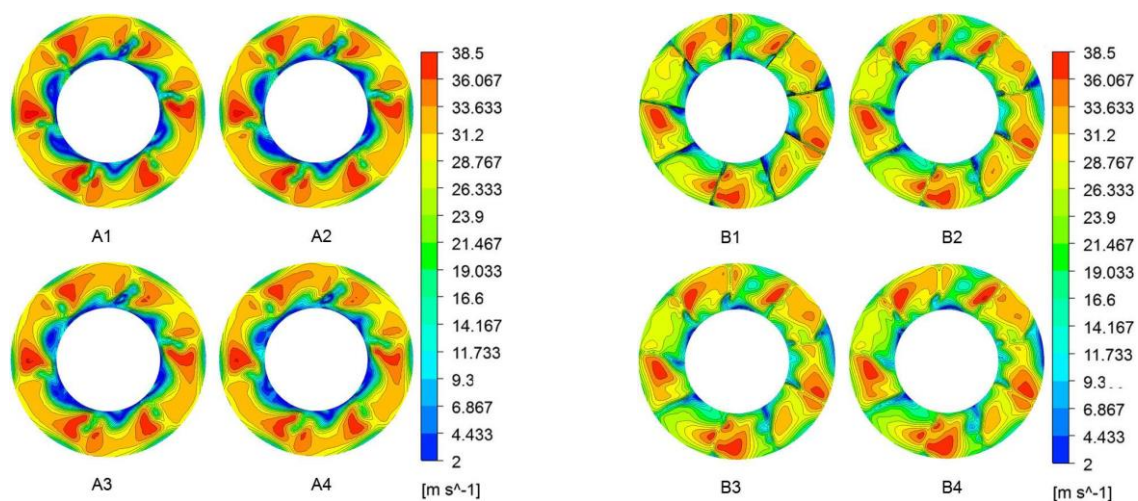


Figure 11. Axial velocity distribution in the impeller-vane inter-stage.

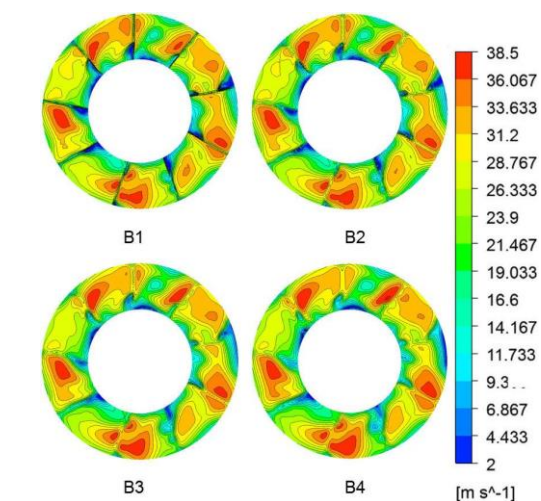


Figure 12. Axial velocity distribution in the vane-impeller inter-stage.

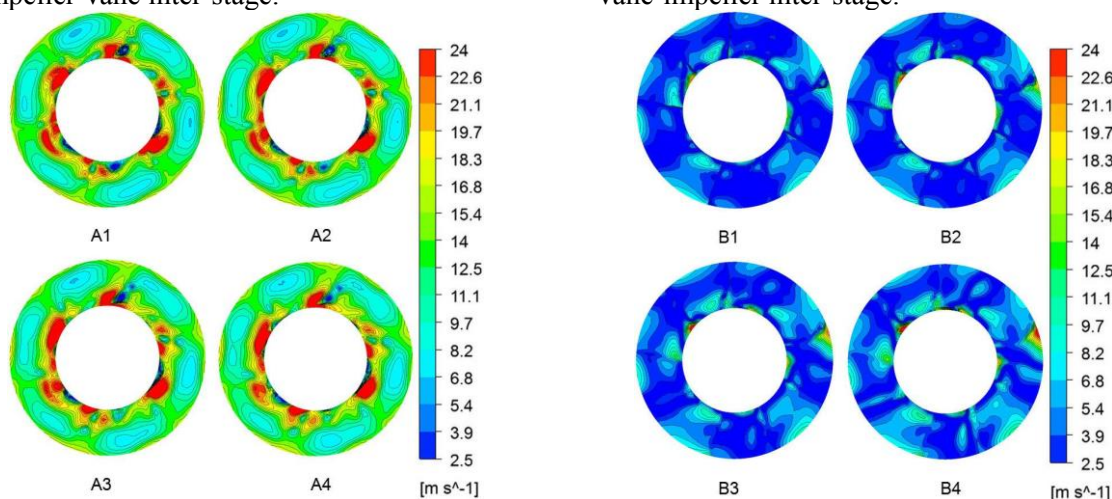


Figure 13. Circumferential velocity distribution in the impeller-vane inter-stage.

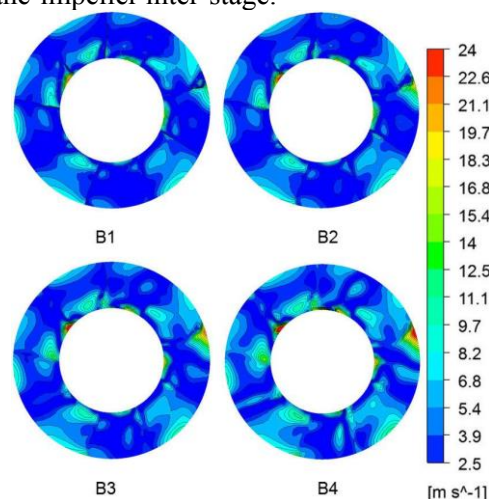


Figure 14. Circumferential velocity distribution in the vane-impeller inter-stage.

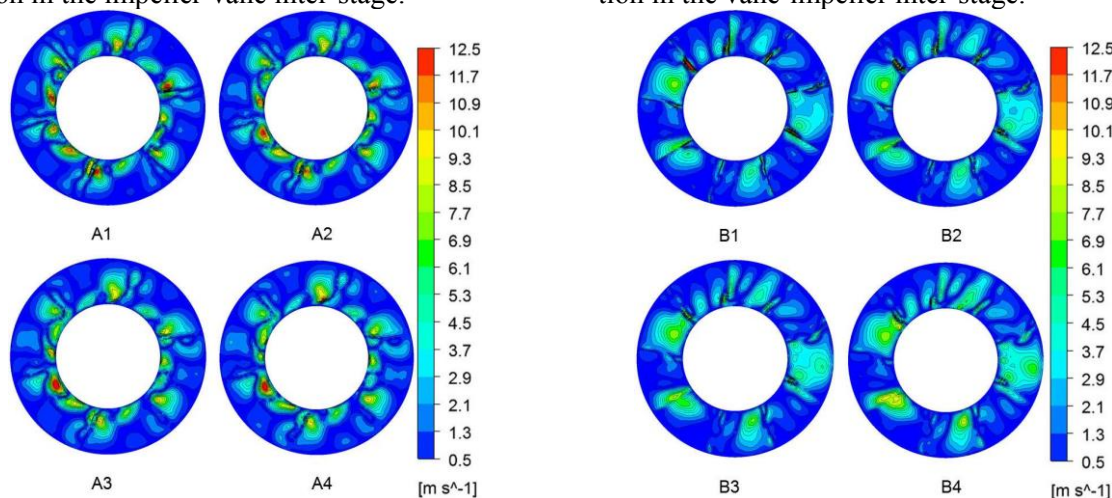


Figure 15. Radial velocity distribution in the

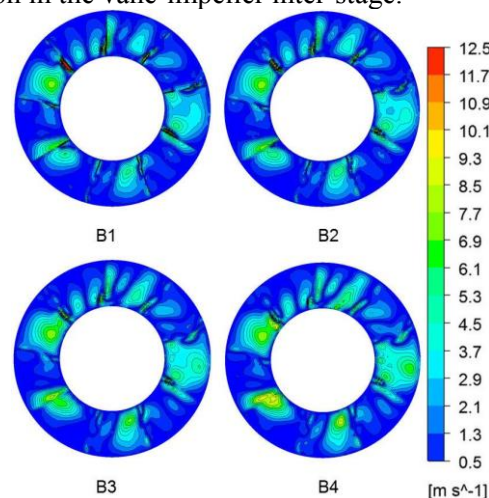
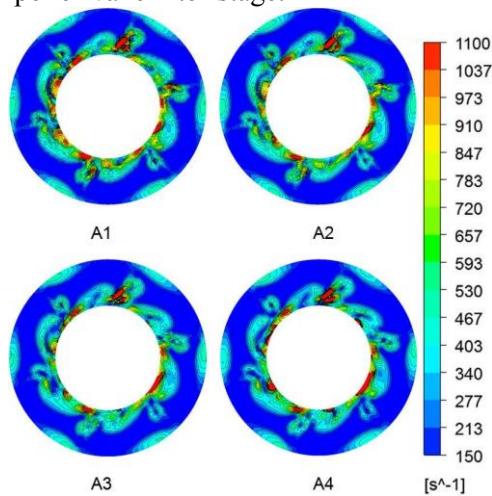
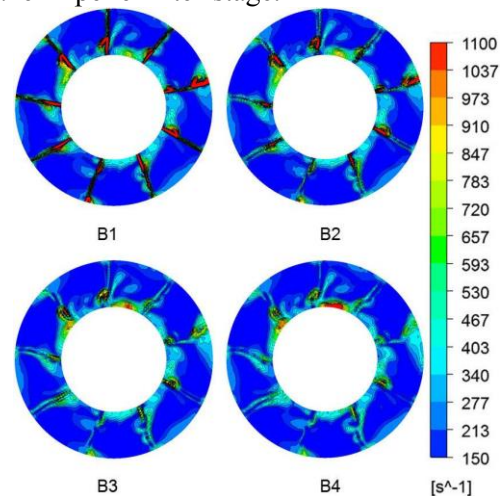


Figure 16. Radial velocity distribution in the

impeller-vane inter-stage.

**Figure 17.** Vorticity distribution in the impeller-vane inter-stage.

vane-impeller inter-stage.

**Figure 18.** Vorticity distribution in the vane-impeller inter-stage.

3.1.1. Distribution of flow field in the impeller-vane inter-stage

From Figure 5, the total pressure distribution cloud chart of the section of the impeller-vane inter-stage can be clearly seen, and the total pressure distribution is symmetric along the circumferential direction, showing the first stage impeller structure characteristics (the number of the first stage impeller blade is 6). There are 6 non mainstream areas and 6 main flow areas. This trend has continued into the leading edge of the inlet. This shows that the characteristics of the first stage impeller are the main influence of the unsteady influence of the impeller-vane inter-stage.

From Figure 7, the static pressure distribution cloud chart of the section of the impeller-vane inter-stage can be seen, and the static pressure distribution is symmetric along the circumferential direction, showing the first stage impeller structure characteristics. There are 6 wake areas and 6 main flow areas. The structural characteristics of the first stage impeller of the A2 to A3 and A4 section are obviously weakened. This shows that the static pressure of the fluid in the A1 and A2 section of the first stage impeller has a major impact on the flows; the A3 and A4 section are influenced by the vane potential flow. From Figure 7 it can be seen that the static pressure in the axial direction is not obvious, and the reverse pressure gradient is very small. This also shows that the influence of the first stage impeller on the flow of the impeller is stronger than that of the vanes.

From Figure 9 the velocity distribution cloud chart of impeller-vane inter-stage and Figure 11 the axial velocity distribution cloud chart of impeller-vane inter-stage which can be clearly seen, the distribution of velocity and axial velocity is the same as that in Figure 5. The structural characteristics of the first stage impeller are presented in each section. There are 6 main areas and 6 non mainstream areas. Figure 13 the section of impeller-vane inter-stage is the velocity chart, which can be clearly seen, 6 main flow areas and 6 non mainstream areas are demonstrated by the section images. The structural characteristics of the first stage impeller are the main position, and the position of the circumferential velocity is at the root of the leaf. From Fig. 15 the radial velocity of section contours of impeller-vane inter-stage which can be clearly seen, there are the 12 main flow areas and 12 non mainstream areas strong or weak showed in the four sections. The number of the first stage impeller blade is 6, which is just 2 times. This shows that the characteristics of the first stage impeller in the radial velocity field of the impeller-vane inter-stage are the main effects. Even in A3 and A4 sections, the structural characteristics of the first stage impeller are obvious, and the radial velocity is disturbed by the vane.

From Figure 17, it is not difficult to find the characteristics of the first stage impeller 6 blades in each section. The vorticity distribution in each section is symmetric, and the influence of the vane is

not affected. It also shows that the first stage impeller has a major influence on the distribution of the vorticity field.

From the above analysis it can be concluded that the total pressure, velocity, circumferential velocity, radial velocity and vorticity in all of the profiles show a strong first level of structural characteristics of the impeller, and the static pressure in the A1 and A2 section also presents a very strong first stage impeller structure characteristics, only the A3, A4 section are influenced by the vane, that is, the influence of the first stage impeller of the impeller-vane inter-stage is the main.

The analysis of the section cloud of the impeller-vane inter-stage can be concluded as follows: the wake interaction has an advantage over potential flow interaction in the impeller-vane inter-stage.

3.1.2. Distribution of flow field in the vane-impeller inter-stage

From Figure 6, the total pressure distribution cloud chart of the section of the vane-impeller inter-stage can be clearly seen, and the total pressure distribution on the B1 and B2 sections show a strong unsteady nature. This is due to the vane-impeller inter-stage flow field in the vane outlet flow not only by the vane wake effect, but also by the effect of the first stage impeller wake. A, B, and C are three distinct asymmetric non mainstream regions from the total pressure contours of B1 section. This is because the mixed results of the first impeller wake which is cut by the vane and the vane wake. The total pressure distribution in B1 and B2 section is symmetric along the circumferential direction, showing vane structure characteristics (The number of vane blade is 9). There are 9 wake areas and 6 main flow areas. While the B3 and B4 sections can also be clearly seen in the structural characteristics of the vanes, the structure features of the second stage impeller has already begun to appear on the section by the influence of the second stage (the number of the second stage impeller blade is 5). There are 5 high pressure zones and 5 low pressure zones. Even the structural features of the impeller on the upstream B1 section are clearly visible.

From Figure 8, the static pressure distribution cloud chart of the section of the vane-impeller inter-stage can be clearly seen. Except of the first stage impeller and vane wake superposition area, the vane blade wake has little influence to the static pressure of the vane-impeller inter-stage. The static pressure distribution along the circumferential direction is symmetrical, and the structure of the second stage impeller is presented. There are 5 high pressure zones and 5 low pressure zones. This shows that the characteristics of the second stage impeller are the main influence of the unsteady influence of the impeller.

From Figure 10 and Figure 12, the velocity distribution cloud chart and axial velocity distribution cloud chart of the section of the vane-impeller inter-stage can be clearly seen. The distribution of velocity and axial velocity is the same as that in Figure 6. Only the B3 and B4 section show a stronger structure of the second stage impeller, Even in the B1 and B2 section, there are 5 regions has the maximum velocity and the axial flow velocity. The structural characteristics of the second stage impeller are presented. From Figure 14 the section circumferential velocity distribution cloud chart of the vane-impeller inter-stage we can see that the structural characteristics of the vane are not. And a clear structure of the second stage impeller can be seen in this section, and this feature closed to the second stage impeller is also more obvious. From Figure 16, the radial velocity distribution cloud chart of the section of the vane-impeller inter-stage can be clearly seen; radial velocity field in each section shows a strong structural characteristic of the second stage impeller. Only in the radial B1 and B2 section, the structure of the vane can be seen not clearly.

From Figure 18, the vorticity distribution cloud chart of the section of the vane-impeller inter-stage can be clearly seen; sections from B1 to B4 have been showing the characteristics of leaf structure. But in the B3 and B4, the structure of the vane is obviously weakened due to the interference of the second stage impeller potential flow. This shows that in the area near the second level of the impeller, the amount of the vortex field is affected by the second stage impeller.

From the above analysis it can be concluded that Static pressure, circumferential velocity and radial velocity in all of the profiles show a strong second level of structural characteristics of the impeller, and the total pressure, velocity, vorticity, in the A1 and A2 section also presents a very strong vane

structure characteristics,. But because of the impact of the second stage impeller, the structural characteristics of the second stage impeller are presented in the A3, A4 section. In relative terms, the influence of second - stage impeller in the inner flow field of the vane-impeller inter-stage is stronger than that of the vanes.

The analysis of the section cloud of the vane-impeller inter-stage can be concluded as follows: the potential flow interaction has an advantage over the wake interaction in the impeller-vane inter-stage. The reason leading to this phenomenon is that the second stage impeller acts on the gas, increases the gas pressure, and produces high adverse pressure gradient.

3.2. Quantitative analysis of distribution of flow field in the inter-stages

To study more clearly on how the distribution of flow field in inter-stage is influenced by the wake interaction and the potential flow interaction. Parameters are extracted in the two inter-stages at the half of Radius, plotted and analyzed. As shown in Figure 19 of position of curve diagram. Method to get Curves is same method to get sections as shown in Figure 4.

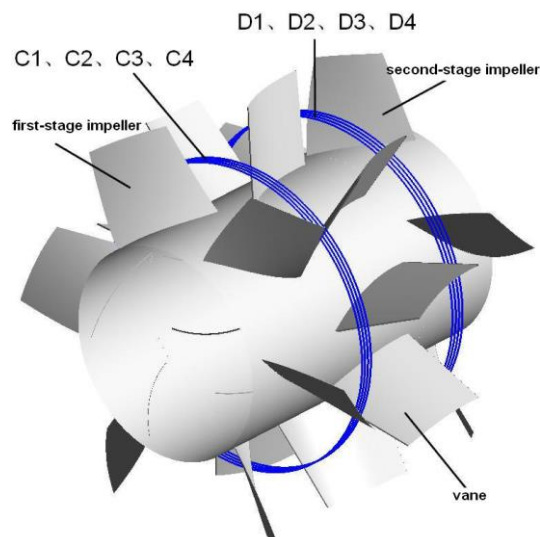


Figure 19. Position of curve schematic diagram

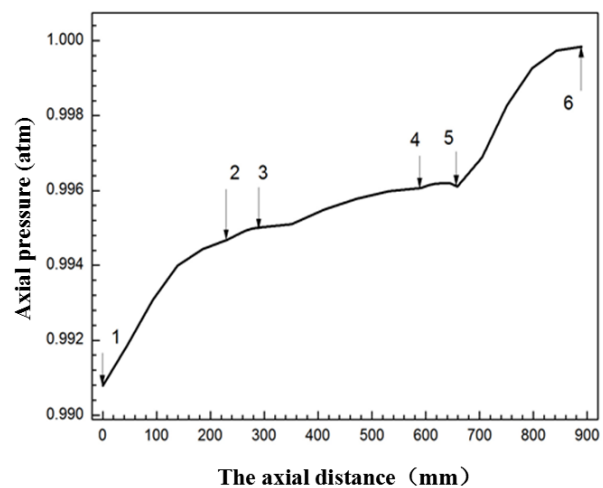


Figure 20. Pressure changes along the axial direction

From the Figure 20 (1-2 is the first-stage impeller, 2-3 is the impeller-vane interstage, 3-4 is vane, 4-5 is the vane-impeller inter-stage, 5-6 is the second-stage impeller), It is obvious that pressure gradient changes gently near the impeller-vane inter-stage, and pressure gradient changes sharply near the vane-impeller inter-stage. That is the reason why the wake interaction produced dominant effect in the impeller-vane inter-stage, the potential flow interaction produced dominant effect in the vane-impeller inter-stage. This is consistent with the qualitative analysis of the foregoing.

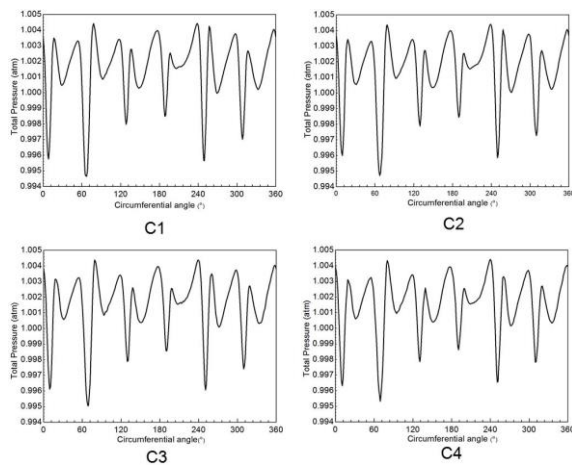


Figure 21. Total pressure distribution along the axial direction in the impeller-vane inter-stage.

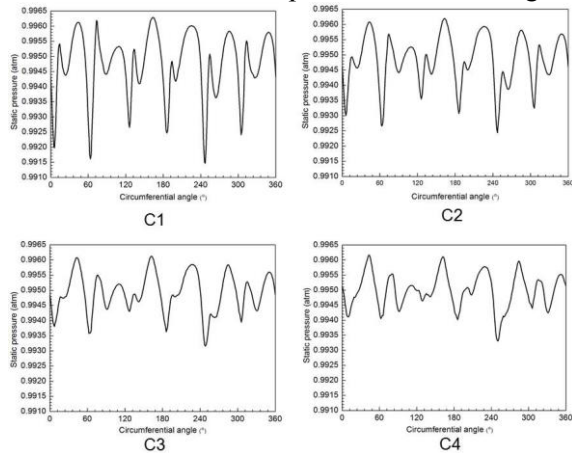


Figure 23. Static pressure distribution along the axial direction in the impeller-vane inter-stage.

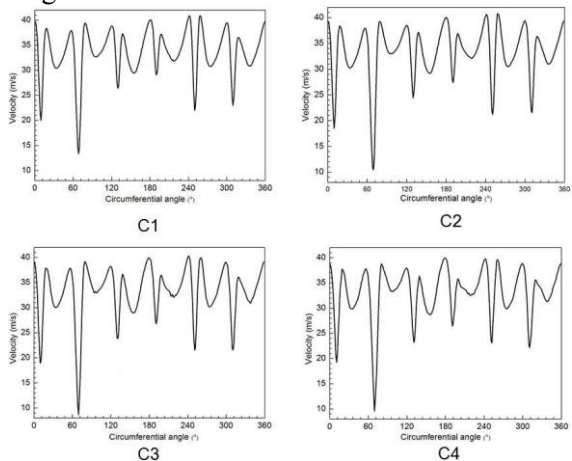


Figure 25. Velocity distribution along the axial direction in the impeller-vane inter-stage.

From the Figure 21, it is obvious that total pressure distribution along the circumferential direction show regularity of 12 peaks and 12 valleys, and has 6 main peaks and 6 main valleys, Presents

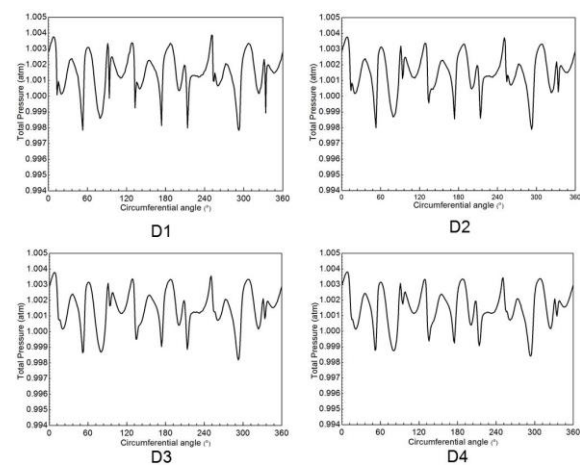


Figure 22. Total pressure distribution along the axial direction in the vane-impeller inter-stage.

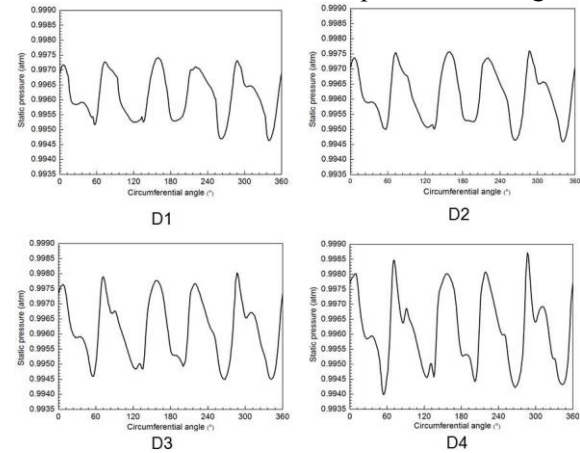


Figure 24. Static pressure distribution along the axial direction in the vane-impeller inter-stage.

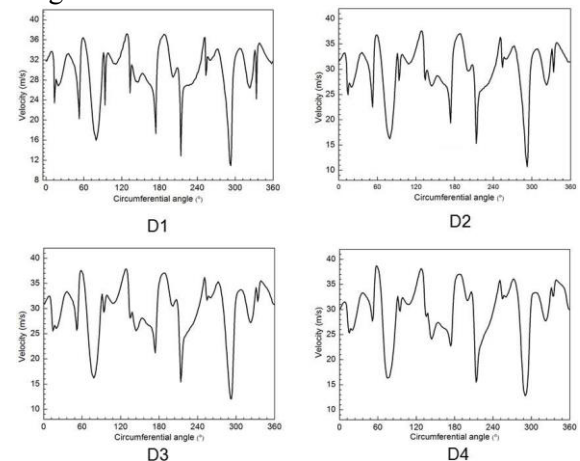


Figure 25. Velocity distribution along the axial direction in the vane-impeller inter-stage.

structural feature of first-stage impeller. From the Figure 22, It shows that total pressure distribution along the circumferential direction is very complicated, But It's obvious that in each section, there are 10 main peaks and 10 main valleys, the number is just about double in blade number of second-stage impeller, so it shows structural feature of second-stage impeller.

From the Figure 23, it is obvious that Static pressure distribution along the circumferential direction, show regularity of 12 peaks and 12 valleys, and have 6 main peaks and 6 main valleys, Presents structural feature of first-stage impeller. From the Figure 24, it is obvious that in each curve, there are 5 peaks and 5 valleys, shows structural feature of second-stage impeller.

From the Figure 25, It is obvious that velocity distribution along the circumferential direction show regularity of 12 peaks and 12 valleys, Presents structural feature of first-stage impeller. From the Figure 26, It shows that total velocity distribution along the circumferential direction is very complicated, But It's obvious that in each section, there are 5 main peaks and 5 main valleys, the number is just same in blade number of second-stage impeller, so it shows structural feature of second-stage impeller.

In summary, total pressure distribution, Static pressure distribution and velocity distribution along the circumferential direction is consistent with the qualitative analysis of the foregoing. Relatively, wake interaction has an advantage over potential flow interaction in the impeller-vane inter-stage; Potential flow interaction has an advantage over wake interaction in the vane-impeller inter-stage.

4. Conclusions

In this paper, Numerical simulation is performed for the internal three-dimensional turbulent flow field in the two-stage axial fan. To analyze how the distribution of flow field in inter-stage is influenced by the wake interaction and the potential flow interaction in the impeller-vane inter-stage and the vane-impeller inter-stage. This paper has the following conclusions:

- (1) The wake interaction has an advantage over potential flow interaction in the impeller-vane inter-stage.
- (2) The potential flow interaction has an advantage over wake interaction in the vane-impeller inter-stage.
- (3) Distribution of flow field in the two inter-stages is determined by the rotating component.

Acknowledgments

This work is supported by Zhejiang Province Key Science and Technology Innovation Team Project (2013TD18) and the National Natural Science Foundation of China (51579224).

References

- [1] Yang J, Qiao W Y, Shi P J, Wang P W. 2012 Primitive staged stator solidity of axial flow turbine to the rotor-stator interaction effects, *Journal of Aerospace Power*, **27**(8):1832-1840 (in Chinese).
- [2] Wang Y f, Hu J, Luo B N, Li C P. 2006 Effects of the Up-stream Blade Wakes on the Spectrum of Rotor Blade Unsteady Surface Pressure, *Journal of Aerospace Power*, **21**(4):693-699 (in Chinese).
- [3] Wu Y D, Zhu X C, Ou Y H, Tian J, Du C H. 2009 Experimental study of flow field of dynamic and static interference, DaLian: The Conference of Pneumatic thermodynamic heat engine of Chinese Society of Engineering Thermophysics (in Chinese).
- [4] Png R, Joselyn H D, Hardin L W, Wagner J H. 1982 Turbine rotor-stator interaction, *Journal of Engineering for Gas Turbines & Power*, **204**(4):729-742.
- [5] Gaetani P, Persico G, Osnaghi C. 2012 Effects of Axial Gap on the Vane-Rotor Interaction in a Low Aspect Ratio Turbine Stage, *Journal of Propulsion & Power*, **26**(2):325-334.
- [6] Mao M M, Zhu Y P, Wang Z Q. 2007 Numerical research on influence of rotor-stator interactions in transonic compressor, *Journal of Aerospace Power*, **22**(9):1468-1474 (in Chinese).

- [7] Qi M X, Feng Z P, Kang Shun, HIRSCH Charles. 2003 Influences of Rotor-stator Interaction on the Performance of Axial-flow Turbine Stages, *Journal of Engineering Thermophysics*, **24**(1):39-42 (in Chinese).
- [8] Yang C, Zhang H Z, Zhao B, Ma Z C Lao D Z. 2015 Analysis of the Interaction Superposition Effect Between Potential Flow and Wake in Axial Compressor Blade Rows, *Journal of Engineering Thermophysics*, **36**(2):269-273 (in Chinese).
- [9] Xiao P and Wang J. 2006 Numerical Study of Interference of Interstage Flows in a Counter rotating Cascade, *Journal of Engineering for Thermal Energy and Power*, **21**(3):249-254 (in Chinese).
- [10] Xiao P. 2005 Steady Numerical Simulation of three-dimensional for the Mutual interference between multi-stage cascades, WuHan: *Huazhong University of Science and Technology* (in Chinese).
- [11] Yang Y. 2013 LES-Based Simulation of Unsteady Flow Within the Axial Gap between Impeller and Diffuser of Axial-flow Pump, JiangSu: *Jiangsu University* (in Chinese).
- [12] Qian Z D, Yang J D, Huai W X. 2007 Numerical simulation And Analysis Of Pressure Pulsation In Francis Hydraulic Turbine With Air Admission, *Journal of Hydrodynamics*, **19**(7):467-472.
- [13] Shih T H, Liou W W, Shabbir A, Yang Z, Zhu J. 1995 A New $k - \varepsilon$ Eddy Viscosity Model For High Reynolds Number Turbulent Flows, *Comput Fluids*, **24**(3):227-238.